

# CHARACTERISTICS OF NON-PREMIXED TURBULENT FLAMES IN MICROGRAVITY

U. Hegde and Z. G. Yuan, National Center for Microgravity Research, Cleveland, OH  
D. P. Stocker, NASA John H. Glenn Research Center, Cleveland, OH  
M. Y. Bahadori, Science and Technology Development Corp., Los Angeles, CA

## INTRODUCTION

This project is concerned with the characteristics of turbulent hydrocarbon (primarily propane) gas-jet diffusion flames in microgravity. A microgravity environment provides the opportunity to study the structure of turbulent diffusion flames under momentum-dominated conditions (large Froude number) at moderate Reynolds number which is a combination not achievable in normal gravity. This paper summarizes progress made since the last workshop<sup>1</sup>. Primarily, the features of flame radiation from microgravity turbulent jet diffusion flames in a reduced gravity environment are described. Tests were conducted for non-premixed, nitrogen-diluted propane flames burning in quiescent air in the NASA Glenn 5.18 Second Zero Gravity Facility. Measured flame radiation from wedge-shaped, axial slices of the flame are compared for microgravity and normal gravity flames. Results from numerical computations of the flame using a  $k-\epsilon$  model for the turbulence are also presented to show the effects of flame radiation on the thermal field.

Flame radiation is an important quantity that is impacted by buoyancy as has been shown in previous studies by the authors<sup>2</sup> and also by Urban et al<sup>3</sup>. It was found that jet diffusion flames burning under microgravity conditions have significantly higher radiative loss (about five to seven times higher) compared to their normal gravity counterparts because of larger flame size in microgravity and larger convective heat loss fraction from the flame in normal gravity. These studies, however, were confined to laminar flames. For the case of turbulent flames, the flame radiation is a function of time and both the time-averaged and time-dependent components are of interest. In this paper, attention is focused primarily on the time-averaged level of the radiation but the turbulent structure of the flame is also assessed from considerations of the radiation power spectra.

## APPROACH

Fuel-nitrogen mixtures are injected into quiescent air through a nozzle (i.d. of 1.65 mm) made of stainless steel tubing. A mixture of 60% propane-40% nitrogen was used. For the results presented here, injection Reynolds number was about 3000. Side views of the flame are imaged by means of video cameras at 30 frames per second. The radiometer assembly utilized for the flame radiation measurements is shown in Fig. 1. It consists of a thermopile radiometer and an optical assembly consisting of a biconvex lens, a plano-cylindrical lens, and a narrow bandpass filter. The filter is centered at 1870 nm which corresponds to a water vapor band. The restriction to the narrow bandpass wavelength range enables the limited field of view desired. This design in conjunction with the placement distance of the radiometer assembly from the nozzle centerline (see Fig. 1) results in a field of view which has an axial extent of approximately 6 mm at the flame centerline. The axial location of the radiometer assembly was varied to obtain the axial distribution of the flame radiation signal. A 16-bit data acquisition system is utilized to record the radiometer signal at sampling rates up to 2000 Hz.

The numerical model utilizes standard turbulent models in conjunction with state relationships for chemistry for predicting the time-averaged flow field. A single step chemical reaction between fuel and oxidizer is assumed. The model solves for pressure, velocity,

temperatures, species concentrations, and turbulent kinetic energy and dissipation rate. The code utilizes a discrete transfer radiation model<sup>4</sup> for CO<sub>2</sub> and H<sub>2</sub>O emissions for radiative transport. This is a grey gas model where the predicted intensity is an integrated intensity over all wavelengths. With this model, the equation for the radiant intensity,  $dI$ , along a path  $ds$  is

$$dI/ds = \alpha I + \beta \sigma T^4/\pi$$

where  $\alpha$  is the net absorption and scattering coefficient,  $\beta$  is the emission coefficient,  $T$  is the local temperature, and  $\sigma$  is Boltzmann's constant. In the present computations, the emission and absorption coefficients are assumed equal at each point in the flow field and scattering in the gas is neglected. The absorption coefficient is a function of the local concentrations of carbon dioxide and water vapor. The above equation must be integrated for a number of rays emanating from a point in the flow field so that the hemispherical solid angle about that point is covered by the rays.

## RESULTS AND DISCUSSION

A typical radiation signal obtained in the drop test for the microgravity flame is shown in Fig. 2 for the final two seconds of the drop. For this test, the axial location of the radiometer was at a  $x/d$  of approximately 150. The radiation signal exhibits a fluctuating behavior consistent with the turbulent nature of the flame. A mean level of the radiation may be obtained during this time frame, but due to the limited time duration of the test, it is not clear whether the signal has achieved a statistically stationary state.

Figure 3 plots the mean measured radiation signal for different axial locations,  $x/L$ , of the radiometer. The results for both the microgravity flame and the corresponding normal gravity flame are shown. It is seen that for the normal gravity flame, the radiation signal increases with axial distance up to approximately the flame tip before beginning to decay. For the microgravity flame, however, the mean radiation signal peaks upstream of the flame tip before decaying. Since radiation is proportional to the fourth power of temperature, the above finding suggests that flame temperatures near the tip for the microgravity flame are reduced compared to the normal gravity case. This is confirmed by the numerical computations as shown in Fig. 4 which plots computed flame centerline temperatures as a function of the distance from the nozzle tip, non-dimensionalized in the same manner as for Fig. 3.

The numerical computations also show that the axial velocity profile for the normal and microgravity flames begin to differ significantly within thirty nozzle diameters axially from the nozzle tip for the flow conditions studied here. This corresponds to roughly 20% of the normal gravity flame height. The effects of buoyant acceleration in the velocity field (for example, higher velocity and velocity gradient) are clearly evident at further downstream locations. This is shown in Fig. 5 which plots the computed radial profile of the axial velocity (non-dimensionalized with respect to the injection velocity) for both normal gravity and microgravity cases at an axial location corresponding to the mean normal-gravity flame height.

Figures 4 and 5 indicate that in normal gravity, a larger fraction of the heat release is lost by convection. This follows by noting that the flame heat release,  $Q$ , can be related to the heat lost by convection downstream of the flame,  $Q_c$ , and the radiative heat loss,  $Q_r$ , as

$$Q = Q_c + Q_r$$

where, for simplicity, conduction is assumed to be negligible compared to the radiative and convective losses. The axial convection of enthalpy downstream of the flame is proportional to the product of velocity and temperature at the flame tip which from Figs. 4 and 5 is greater for

the normal gravity case. Consequently, radiative transfer becomes more dominant in the absence of buoyancy.

The microgravity flame radiation power spectra for three locations,  $x/d = 30, 120$  and  $180$ , respectively are shown in Fig. 6. At the lowest location, the spectral magnitude levels are the smallest of the three. Further downstream, at  $x/d = 120$  (in the region where the time-averaged radiation levels reaches a maximum), the magnitude of the spectra increases over the entire frequency range of interest. This indicates an increase in the magnitude of the turbulent fluctuations. However, further downstream, at  $x/d = 180$ , while the lower frequency components (up to 30 Hz, approximately) are of similar magnitude compared to those at  $x/d = 120$ , the higher frequency components are of smaller magnitude. This result is consistent with computations that indicate that the axial velocity near the flame tip of the microgravity flame is only a few percent of the injection velocity i.e., an order of magnitude lower. Hence, the local Reynolds number based upon the local centerline velocity is also expected to decay significantly. Furthermore, if it is assumed that the local turbulent velocity magnitude scales with the local centerline velocity, and that the local integral length scales with the local flame width which is relatively invariant over the flame length, then it is clear that the local turbulent Reynolds number,  $Re_T$ , also decays. The smallest scale of turbulence, that is, the dissipation length scale, varies as  $Re_T^{-0.75}$  [e.g. Tennekes and Lumley<sup>5</sup>] indicating that the size of the smallest scales increases with increasing distance along the flame (since  $Re_T$  decreases). This is also consistent with turbulence dissipation behavior. The turbulence dissipation is of order  $u'/l$  where  $u'$  is the turbulent velocity fluctuation magnitude and  $l$  is the integral length scale [e.g., Spalding<sup>6</sup>]. This is a measure of the highest frequencies (i.e., the smallest scales) in the turbulent spectrum. The integral length scale is expected to be relatively invariant over the flame length whereas  $u'$  will scale with the mean velocity which decreases axially. Thus,  $u'/l$  is expected to decrease downstream indicating a decrease in the highest frequencies and an increase in the size of the smallest scales.

The normal gravity flame radiation power spectra for three locations,  $x/d = 30, 90$ , and  $120$ , respectively are shown in Fig. 7. At the lowest location, there is a strong peak at a frequency of approximately 14 Hz which may be related to the flame flicker observed at lower Reynolds numbers. Further downstream (e.g.,  $x/d = 90$ ), the spectra broaden out, and the spectral levels are higher at all of the frequencies. At  $x/d = 120$ , which is near the observed flame tip, the overall fluctuation amplitudes are larger and the frequency range of the turbulence is not reduced.

#### ACKNOWLEDGEMENT

This work was supported by NASA under cooperative agreement NCC3-544 and contract NAS3-98032. The assistance of Mr. Dennis Thompson, Zero-G Facility manager at NASA Glenn Research Center, in the conduct of the tests is greatly appreciated. Jonathan Sakai of the University of Dayton assisted with the numerical code computations during internships at NASA Glenn and NCMR.

#### REFERENCES

1. Hegde, U., Yuan, Z. G., Stocker, D. P., and Bahadori, M. Y. [1999] Characteristics of Non-Premixed Turbulent Flames in Microgravity, Fifth International Microgravity Combustion Workshop, Cleveland, OH.
2. Bahadori, M. Y., Stocker, D. P., Vaughan, D. F., Zhou, L., and Edelman, R. B. [1993] in Modern Developments in Energy, Combustion, and Spectroscopy (Williams, F. A., Oppenheim, A. K., Olfe, D. B., and Lapp, M., Eds.), Pergamon Press, Oxford, pp. 49-66.
3. Urban, D. L., Yuan, Z. G., Sunderland, P. B., Linteris, G. T., Voss, J. E., Lin, K. C., Dai, Z., Sun, K., and Faeth, G. M. [1998] *AIJA J*, vol. 36, pp. 1346-1360.
4. Siegel, R., and Howell, J. [1981] *Thermal Radiation Heat Transfer*, Second Edition, McGraw-Hill.
5. Tennekes, H. and Lumley, J. L. (1977). *A First Course in Turbulence*. Fourth Printing, The MIT Press, Cambridge, Massachusetts.
6. Spalding, D. B. (1971) *Chem. Eng. Sci.*, vol. 26, pp. 95-114.

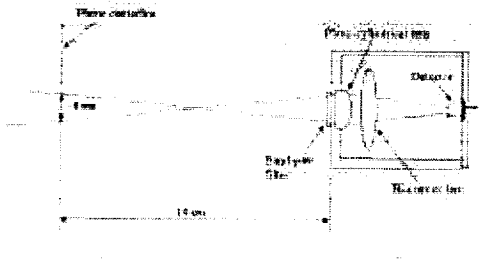


Fig 1 Narrow-view radiometer assembly

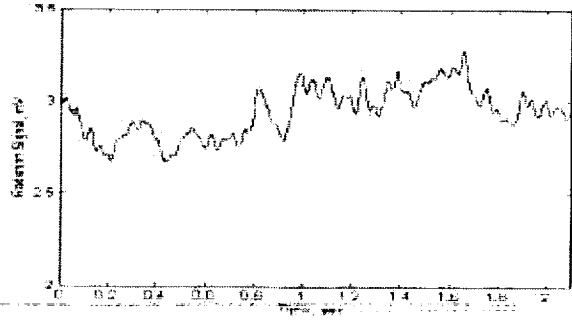


Fig 2 Typical measured radiometer signal during the final 2 seconds of the drop test

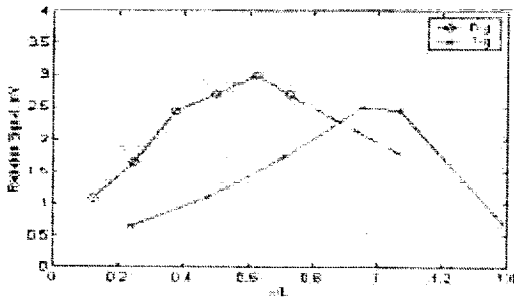


Fig 3 Measured radiation signal as a function of non-dimensional axial location

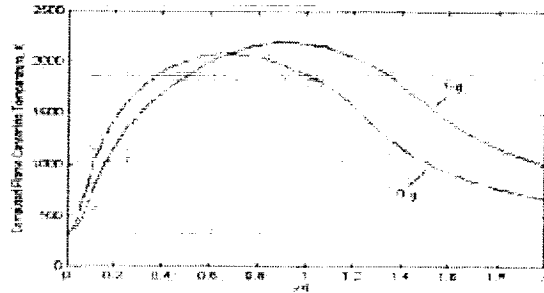


Fig 4 Computed centerline temperature distribution

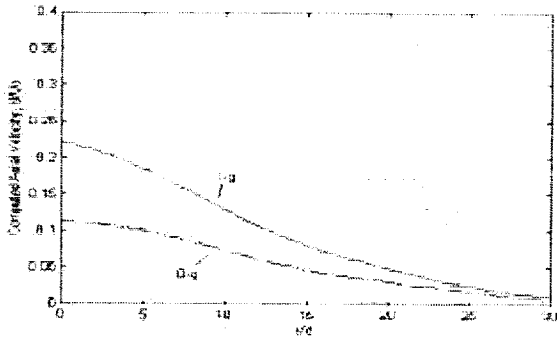


Fig 5 Computed radial profile of axial velocity at an axial location corresponding to the normal gravity flame tip

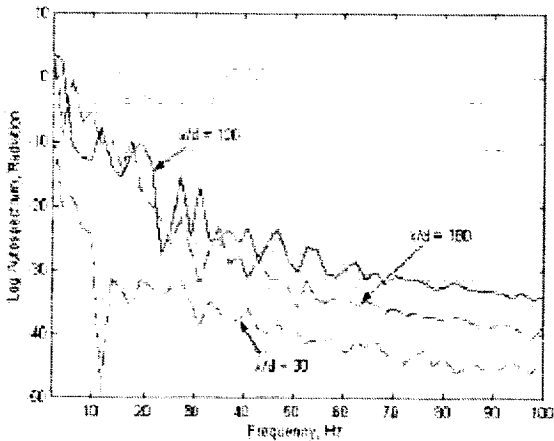


Fig 6 Measured log autospectra of microgravity flame radiation

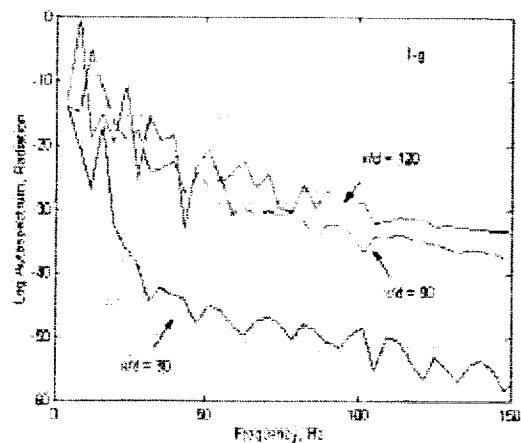


Fig 7 Measured log autospectra of normal gravity flame radiation